land

MDPI

Article

The Thickness of Talus Deposits in the Periglacial Area of SW Spitsbergen (Fugleberget Mountainside) in the Light of Slope Development Theories

Piotr Dolnicki [1] and Mariusz Grabiec [2,*]

[1] Department of Tourism and Regional Studies, Institute of Geography, Pedagogical University of Krakow, Podchorążych 2, 30-084 Krakow, Poland; piotr.dolnicki@up.krakow.pl
[2] Institute of Earth Sciences, Faculty of Natural Sciences, University of Silesia in Katowice, Będzińska 60, 41-200 Sosnowiec, Poland
* Correspondence: mariusz.grabiec@us.edu.pl

Abstract: Periglacial slopes are susceptible to recent climate change. The rate of morphogenetic processes depends on numerous factors. The most important of these is the warming of the air and ground, increased precipitation (extreme rainfall in particular), and the rate of snow cover decay. The dynamics of these processes may effectively modify contemporary slope development models. The paper shows the structure of selected talus slopes on a Fugleberget mountainside, based on field observations and radar (GPR) soundings. The results are then compared to classical slope models. The radar survey in April and May 2014 used a RAMAC CU II Malå GeoScience system equipped with a 30 MHz RTA antenna (Rough Terrain Antenna). Five GPR profiles of different lengths were obtained along the talus axes, transversally on Fugleberget and partly on the Hansbreen lateral moraine. According to the radar soundings, the maximum thickness of the debris deposits is 25–30 m. The thickness of the weathered material increases towards the talus cone's terminal part, and debris deposits overlap marine sediments. The talus slopes' morphometry shows that their current forms differ from standard slope models, which may be due to the significant acceleration of geomorphic processes resulting from climate change, including rapid warming in the last four decades.

Keywords: talus cone; GPR; Svalbard; slope development model; debris

Citation: Dolnicki, P.; Grabiec, M. The Thickness of Talus Deposits in the Periglacial Area of SW Spitsbergen (Fugleberget Mountainside) in the Light of Slope Development Theories. *Land* **2022**, *11*, 209. https://doi.org/10.3390/land11020209

Academic Editor: Jesús Ruiz-Fernández

Received: 29 October 2021
Accepted: 20 January 2022
Published: 28 January 2022

1. Introduction

The periglacial concept was first introduced by Łoziński [1]. Initially used only with reference to the Pleistocene, it was later extended to cover present-day regions with climate specific to areas adjacent to ice caps, glaciers, and high-mountain areas. The term "periglacial zone" has two primary meanings. The first implies a limited zone directly adjoining a glacier, which has brought about specific climatic changes. In the second, broader sense, the periglacial zone is a separate area between the tree line and the snow line, not necessarily climatically or spatially related to a glaciated area, e.g., the permafrost in Siberia [2,3]. Southern Spitsbergen, the area of this research, is an example of a contemporary periglacial zone. The term "cryosphere" is also inherent to the existence of permafrost [4]. It is a layer formed by sub-zero temperatures dependent on the winter season's duration [5]. The extents of the permafrost, periglacial zone, and cryosphere were determined based on climatic criteria [5]. Morphogenetic zones are distinguishable from the close relationship between geomorphological processes and climate. Spitsbergen belongs to the frost-rubble zone [6,7]. The regions within that zone are susceptible to recent climate changes, which in that part of the Arctic are reflected by increased air temperatures, a thicker active layer of permafrost [8–10], a larger sum of rainfall, increased ratio of liquid fraction in total precipitation [11] and faster snow cover decline [12]. Such evident climate changes should be reflected in the evolution of the surface morphology and the rate of

the processes forming it. Morphogenetic changes on periglacial slopes are a common and widely described phenomenon in the Arctic.

In Svalbard, the consequences of catastrophic floods, which activated landslides, endangering the inhabitants in the Longyearbyen region in 1972, were described by Thiedig and Kresling [13] and Rapp [14]. Jahn [15] classified the processes on periglacial slopes in Longyeardallen, which included the formation of erosion-carved troughs and landslides. The formation of erosion-carved troughs on slopes in the Hornsund region was described by Haas et al. [16]. The relationship between slope processes and the ground temperature was studied at Kapp Linné [17]. At present, intensive research is in progress on the morphodynamics of slopes altered by heavy rainfalls causing landslides, thus posing a threat to the inhabitants of Longyearbyen. The slope processes in the periglacial zone are connected with climate changes. This, however, is a generalization, and both the climatic background as well as the structures and dynamics of the slopes need to be studied.

Undoubtedly, contemporary periglacial processes modeling mountain slopes differ regionally [18,19]. Similar conclusions were presented by Van Steijn et al. [20]. He defined the cause of the movement of weathered material within the cones as "a variety of processes" that should be interpreted individually in each analyzed area. The diversity of the processes shaping the debris cones is also the effect of the periglacial zone's broad definition. Processes modeling slopes in such different climatic conditions affect the shape of the talus cone and its formation mechanism.

Hales and Roering [21], while researching in the New Zealand Alps, pointed to the local relief and erosion and the slope inclination as the most significant factors. In turn, in the Rocky Mountains, Moore et al. [22] found that tectonic stress is a critical factor in the movement of weathered material.

The purpose of this research was to characterize specific talus cones on Fugleberget, based on field observations (including ground penetrating radar—GPR investigations). Radar surveys aimed to determine the thickness of debris cones and their internal structure, which will then be interpreted concerning the surface morphology of the cones identified during geomorphological reconnaissance and analysis of photographic material and observations using UAVs. In order to recognize the morphogenesis of Fugleberget debris cones, they will be presented with the reference forms of talus slopes developing in the periglacial environment according to the French [23] and Ballantyne and Harris [24] classifications. The screes will also be described in terms of their morphodynamics and activity concerning the climate changes observed in the southern Svalbard region in the last four decades.

1.1. Study Area

The study area is located in the southwestern part of Svalbard (Figure 1). Ariekammen (517 m a.s.l.) and Fugleberget (569 m a.s.l.), analyzed in detail, are mountains built from gneisses and crystalline schists with marble inclusions. This series belongs to the lowest part of the Hecla Hoek formation [25]. Its physical properties are essential in the context of weathering and denudation processes [26]. The rocky debris and the mixture of debris and clay are characteristic landforms in the slope deposit zone.

Situated near the Polish Polar Station, in a region where interdisciplinary environmental research is conducted, the study area acts as a laboratory for periglacial research and studies of morphogenetic processes and terrestrial ecosystems. Four talus slopes with a southerly exposure, designated I, II, III, and IV, were studied in detail from east to west (Figure 1). The altitudes of Taluses I-III range between 20 and 150 m a.s.l., whereas "Talus IV" appears at 90 m a.s.l. and terminates at 15 m a.s.l.

"Talus I", covering an area of ca 0.02 km^2, is the easternmost one, close to the Hansbreen lateral moraine. Its slope inclinations are the steepest, varying from 28° in the upper part to 19° at the foot (25° on average). This talus cone is subject to the most significant morphodynamic activity and has the sparsest vegetation coverage.

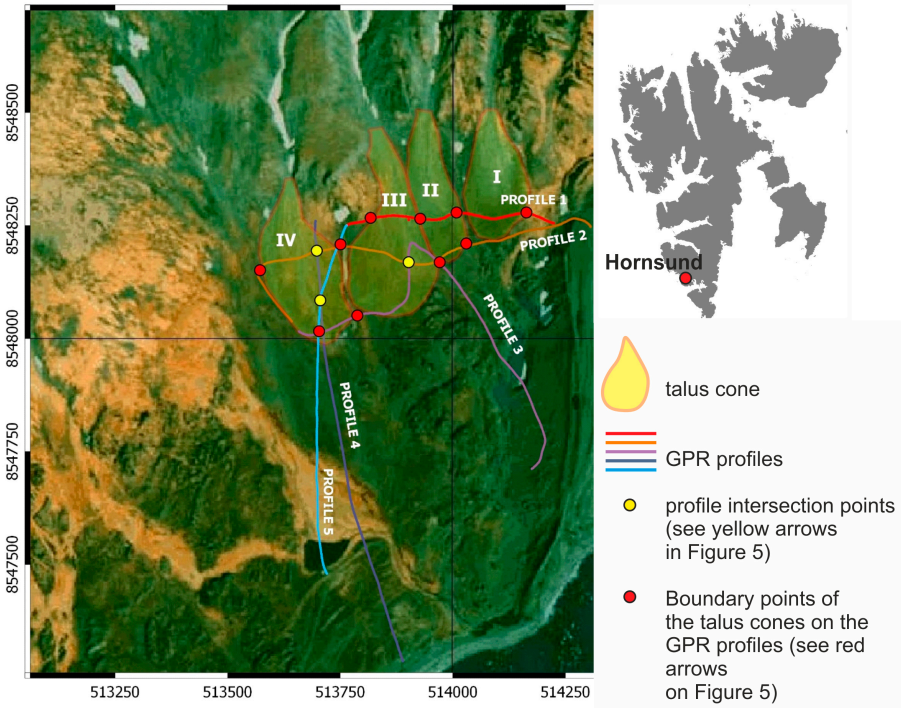

Figure 1. Study area and the location of the GPR surveys (background: orthoimage of [27], courtesy of L. Kolondra).

Situated farther to the west, "Talus II" and "Talus III" are 0.02 km^2 in area and have an average slope inclination of 16°. The geomorphological activity of meteoric water and meltwater has formed distinct erosion gutters (up to 1 m deep) in the middle part of the cones. The lower parts of both talus cones rest on raised terrace sediments and are covered by dense solifluction lobes. "Talus III" is sparsely vegetated, primarily by tundra lichen growing on the lower slope section.

The westernmost "Talus IV" covers an area of ca 0.03 km^2 and exhibits the slightest inclination, increasing the upslope from 4° to 15° (8° on average). This talus cone is geomorphologically less active (no distinct erosion forms), and vegetation succession is prolonged. The slope deposits (debris) gradually evolve into a raised sea terrace in the lower part of the talus cone. This area is covered by wet moss tundra. The grain fraction of the rock deposits covering all four talus slopes generally increases with elevation, from silt to boulders larger than 0.1 m in diameter.

1.2. Climatic Conditions

Climatic conditions constitute a background and reference to studying the evolution of permafrost on mountain slopes and changes in their morphology [28]. In combination with orography, climatic conditions determine the type and trend of morphogenetic processes. The subpolar climate is quite different in the northern and southern parts of Svalbard. Influenced by the warm North Atlantic Current, southern Spitsbergen experiences the typical features of a maritime climate. The main factors affecting the weather conditions are the incoming solar radiation, the atmospheric circulation, and the variable snow cover duration, reflecting a significant portion of the solar radiation.

The most important feature of the light conditions in Svalbard is that there are polar nights and days. The polar day in southern Spitsbergen lasts 117 days [29]. Theoretically, the maximum light intensity should occur in early July, when the sun dominates the horizon at an elevation of 36°. However, the frequent cloud cover occurring in that period makes May the month with the highest solar radiation [29]. This, however, is not important as regards the processes taking place on the slopes because, in May, there is usually a uniform snow cover of substantial thickness. In Hornsund, the polar night lasts 104 days and is

shorter than the polar day by about two weeks. This is the result of refraction, which makes the sun visible over the horizon, although it is already below the horizon. The intensity of direct solar radiation depends on the sun's altitude above the horizon and, consequently, on the sun's rays' angle. A 30° angle of incidence gives a 389 Wm^{-2} to a flat surface [29]. The largest monthly amounts of total solar radiation are recorded in May and July. Like insolation, radiation significantly impacts the thermal state of the active permafrost layer and on morphogenetic processes when slopes are snow-free.

In a year, two stationary pressure centers—the Icelandic Low and the Greenland High/Anticyclone [30]—play the most crucial part in shaping the weather conditions. During autumn and winter, cyclonic situations are prevalent: they are associated with the Icelandic Low, the trough of which reaches as far as the Kara Sea, shaping the weather in southern Spitsbergen for >50% of days from September to March. Low-pressure centers are carrying warm; moist air moves north-eastwards rapidly along the axis of that trough [31], which results in increased precipitation [11]. The situation changes in spring. The expanding, poleward moving Greenlandic High then affects the weather in southern Spitsbergen. Its impact is particularly evident in May—the month when anticyclonic situations are dominant: these influence the weather during more than 60% of days. During summer, highs and lows occur by turns. Cyclonic situations generally prevail during the year, determining the weather in southern Spitsbergen for more than 57.1% of days, whereas anticyclonic situations stay during more than 40% of days [30,32].

Radiation and air circulation determine basic meteorological conditions, such as air temperature, precipitation, and sunshine duration, which mediate changes in ground temperature. The temporal variation in the factors governing soil's thermal properties determines the increase or decline of permafrost on slopes and the morphogenetic intensity of rain- and meltwater. The mean annual temperature for 1990–2014 was −3.4 °C, exhibiting a rising trend (Figure 2). The coldest year (−5.3 °C) was 1993, and the warmest one (−1.1 °C) was 2012.

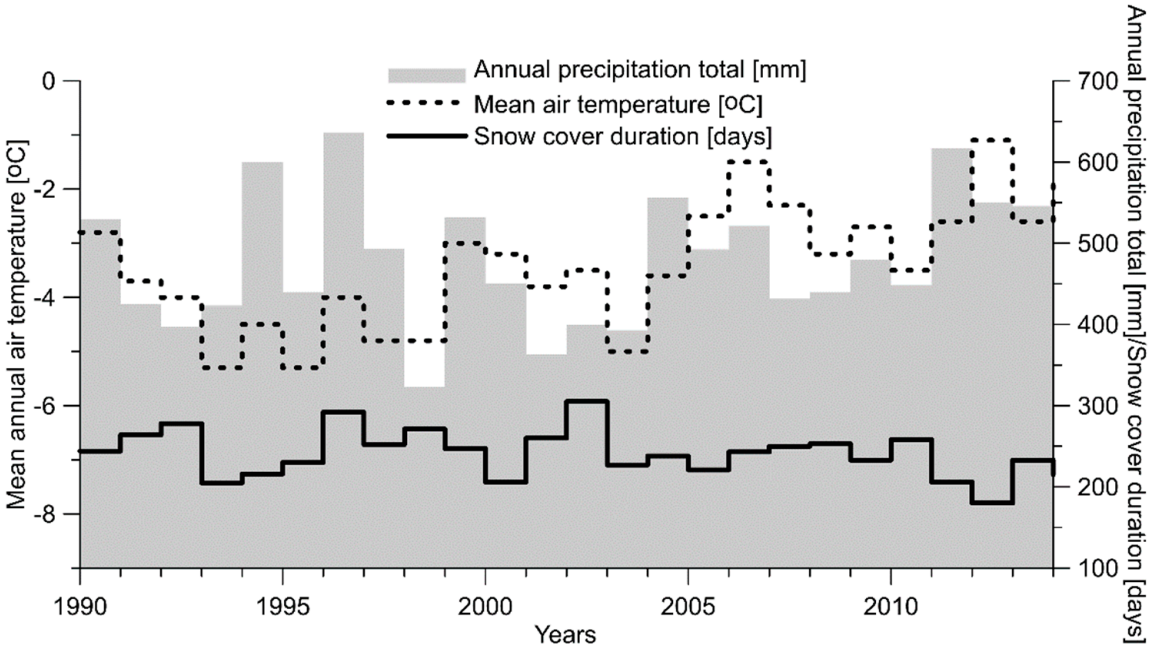

Figure 2. Climatic conditions 1990–2014 at the Polish Polar Station weather station in Hornsund (https://monitoring-hornsund.igf.edu.pl, (accessed on 29 October 2021)): mean annual air temperature, annual precipitation, number of days with snow cover.

The characteristic of polar regions is the small amount of precipitation due to the low moisture content in the air. Nevertheless, there are considerable amounts of precipitation in Hornsund, strongly influenced by the atmospheric circulation from the Norwegian and

Greenland Seas [11,12]. Between 1990 and 2014, the mean annual precipitation was 481 mm (Figure 2). The highest annual precipitation (636 mm) was recorded in 1996 and the lowest (323 mm) in 1998. The highest amounts of precipitation were recorded in autumn (about 33% of the annual total). From 1990 to 2014, there was a statistically significant increasing trend in precipitation.

1.3. Snow Cover

Snow cover in southern Spitsbergen is determined by three factors: solid precipitation, winds able to redeposit snow, and short-term thaws in winter leading to the formation of ice crusts which prevent the snow cover from being blown away [33]. The snow cover on the slopes usually appears at the end of September and remains until June. Initially, it is relatively unstable but gains stability during the polar night. Analysis of the data from 1990–2014 shows that the snow cover around the Polish Polar Station persists for 241 days on average, i.e., two-thirds of the year (Figure 2). The snow cover on the slopes persists longer than on the coastal plains, while in the couloirs over the talus cones, it remains until late July–early August. The photographs in Figure 3 compare the snow patches extent on Fugleberget in July over 17 years. The snow deposited in depressions and rainwater feeds the local streams, which participate in the morphogenetic changes on the talus deposits.

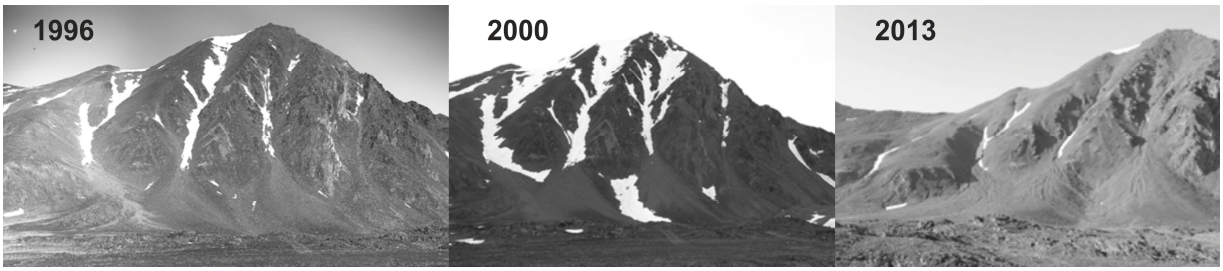

Figure 3. Snow cover on the slopes of Fugleberget in the first half of July in different years (Photo: Archives of the Institute of Earth Sciences, the University of Silesia in Katowice).

1.4. Active Layer

Analysis of the ground temperature at depths of 0.5 and 1.0 m shows a similar increasing trend between 1990 and 2014 (Figure 4). The consequence of increasing ground temperature is the progressive thawing of the permafrost. Long-term thawing of permafrost and the increasing snow cover depth significantly affect talus slopes' morphological processes.

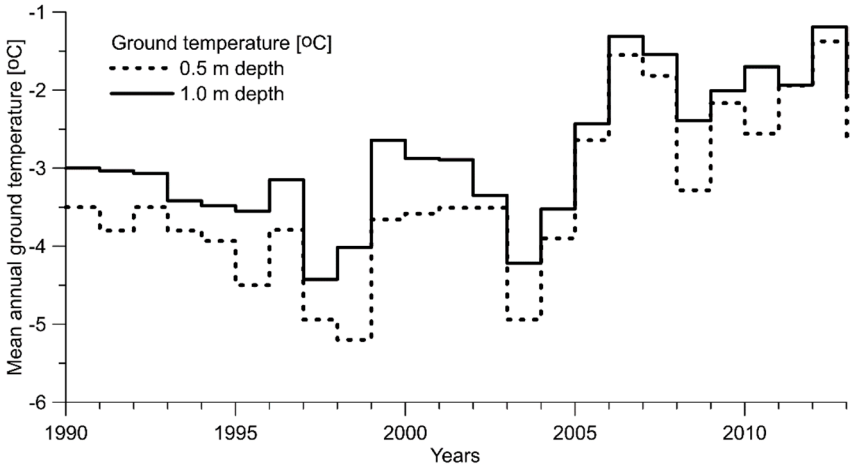

Figure 4. Annual average ground temperature 1990–2013 at the Polish Polar Station weather station in Hornsund (https://monitoring-hornsund.igf.edu.pl, (accessed on 29 October 2021)).

2. Methods

When analyzing the features of the debris cover on talus slopes, especially its thickness and structure, we apply radar sounding as an exceptionally efficient technique [34–39]. To identify the internal structure of talus deposits, two series of radar surveys were carried out in April and May 2014. The research embraced the lower parts of the southern slope of Fugleberget, part of the Fuglebergsletta coastal plain, and the western part of the Hansbreen lateral moraine. Eleven GPR profiles were obtained (five in the April series and six in the May series), 7.8 km in total. Five of these profiles were used in the subsequent analysis to identify the structure of the talus deposits. The measurements were performed using the Malå GeoScience CUII impulse radar system with an RTA-type antenna and a center frequency of 30 MHz. In the April series of measurements, the GPR antenna was towed behind a snowmobile moving at a constant 20 km/h. In May, the GRP system was carried by an operator traversing the snow on skis. Therefore, while maintaining a constant time interval of 0.2 s for triggering the radar pulses, the distance between the traces varied between 0.9 m (April) and 0.1 m (May). The soundings also differed regarding the assumed time window (between 766 and 1317 ns). Still, the ground penetration level enabled the debris covering the bottom of the slopes to be identified each time. The GPR traces were positioned using the GNSS system operating in kinematic mode. The estimated mean error for determining the XYZ positions of GPR traces was 0.2 m. The GPR data obtained were then processed using DC removal, time zero adjustment, mean trace subtraction, bandpass filtering, and topographic correction. As recommended for most talus deposits, a radio-wave velocity of 10 cm ns^{-1} was used for the time-to-depth conversion [35]. A digital terrain model was used to characterize the morphometry of the slopes. This model was obtained based on terrestrial laser scanning (TLS) performed on 24 August 2015 and 6 July 2016 using a Riegl VZ-6000 long-range laser scanner. Due to its long working range and data acquisition speed, this TLS model has been widely used in geomorphological [40–42] and glaciological research [42,43]. The survey was performed at a pulse repetition rate of 50 kHz. The vertical and horizontal angular resolution was between 0.008° and 0.025°, which corresponds to a spatial resolution of about 0.07–0.22 m at a distance of 500 m from the scanner. Thus, the point clouds were initially processed using RiSCAN-PRO software, then exported to a LAS format, based on which the digital terrain model was generated using Global Mapper software.

3. Results

3.1. "Talus I"

The analysis of the internal structure and thickness of "Talus I" (Figure 1) is based on the initial section of GPR profile 1 (Figure 5a). The superficial layer is characterized by low reflectiveness and indistinct layering with a maximum thickness of 9 m. The eastern and western lateral parts of "Talus I" are highly reflective and layered. In the middle part of the talus cone, a visible zone yields an attenuated radar signal, surrounded by a distinct, 20 m thick layer of material bordered by the bedrock.

3.2. "Talus II"

The analysis of the internal composition and depth of "Talus II" (Figure 1) is based on the middle section of "Profile 1" and part of "Profile 2" (Figure 5a,b). "Profile 1" shows layering at the foot of the talus slope and its distinct reflectivity. The thickness of the layer varies from 10 m on the eastern side to 17 m in the western section, and the bedrock elevation rises along with the profile. "Profile 2" characterizes the talus cone frontal parts as a layer with a chaotic diffraction pattern of maximum thickness 13 m, overlapped in the western part by "Talus III".

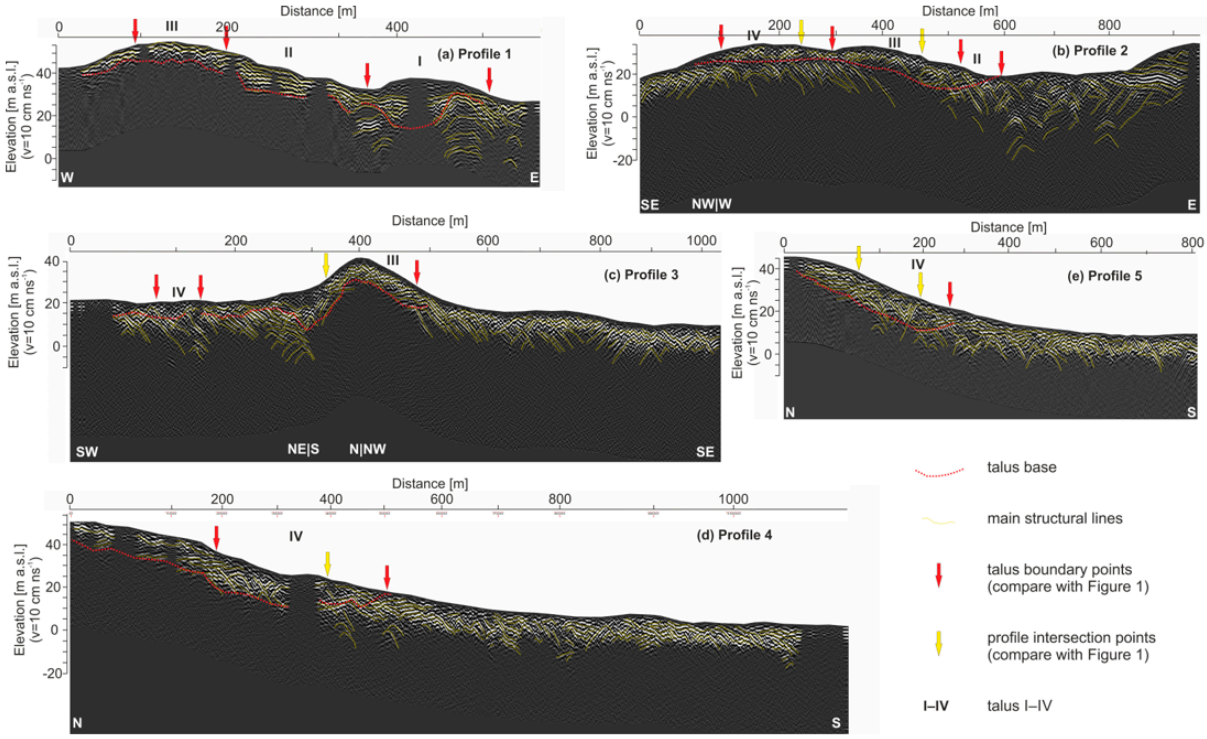

Figure 5. GPR profiles (30 MHz) of the talus slope on the Fugleberget mountainside. (**a**)–Profile 1, (**b**)–Profile 2, (**c**)–Profile 3, (**d**)–Profile 4, (**e**)–Profile 5. See Figure 1 for the location of Profiles 1–5.

3.3. "Talus III"

The structure and depth of "Talus III" (Figure 1) are identified from the analysis of the initial part of "Profile 1" and the middle sections of "Profile 2" and "Profile 3" (Figure 5a–c). A two-layered, 12–14 m thick structure is perceptible in the talus slope upper part ("Profile 1"). The top 7–9 m thick, highly reflective layer overlies a 5 m thick layer with weaker reflective properties. The middle part of "Talus III" is characterized by "Profile 2". The eastern section of "Talus III" forms an up to 17 m thick layer of irregularly structured multireflective material overlapping "Talus II". In the middle part of "Profile 2", which crosses "Talus III", the slope deposits reach a total depth of 25 m, including the top 2 m layer of lower reflectivity. In the NW part of "Talus III", layers are emerging towards "Talus IV". According to "Profile 3", the frontal part of the talus cone is up to 13 m thick in the SE and SW sections. The top layer gradually appears towards the talus slope axis with a clear reflection horizon 7 m below the surface. In the middle part of the cone, the GPR survey shows a chaotic, non-layered structure down to 10 m.

3.4. "Talus IV"

The description of "Talus IV" (Figure 1) is based on a combination of four GPR profiles. "Profile 2" and "Profile 3" run perpendicularly to the talus slope axis in its upper and lower parts, respectively. On the other hand, "Profile 4" and "Profile 5" generally lie parallel to the cone axis (Figure 5b–e). The surficial layer in the talus slope elevated part consists of chaotic material with a multi-reflective structure at a maximum of 9 m thick in the central section. The underlying layered structure is inclined east- and south-eastwards and varies in thickness from 15 m on the talus cone margin to 7 m in its central part. The debris covering this cone part varies in thickness from 19 m in its lateral parts to 16 m along the talus slope axis. The structure of the frontal part of "Talus IV" is quite similar to that of the upper section. A deeper layered structure from 9 to 23 m in thickness and sloping south-westwards (towards "Talus III") is overlain by a 4 m thick surficial layer with a chaotic multi-reflection pattern. Based on "Profile 4", the structure of the deposits along the axis of "Talus IV" is layered at different depths, varying from 11 m in the frontal part to

20 m in the middle of the slope thinning to 12 m in the upper section. "Profile 5" shows analogous depths of slope deposits, starting from an up to 9 m thick layered structure in the lower part, through a chaotic form up to 19 m thick, and ending in an 11 m deep section with a layered pattern in the upper part.

4. Discussion

4.1. Geometry and Internal Structure of the Talus Slopes

From the results of the GPR measurements conducted on the talus slopes of Fugleberget, one can interpret the thickness and structure of the debris material and the geometry of the forms. The active "Talus I" is rich in water-saturated silt along its axis. This zone is characterized by a shallow penetration of the radio waves, typical of highly conductive materials. This may herald the early spring activation of the drainage of sub-snow water along the talus slope. Drainage troughs carved in the cones are often seen after snow decay (Figure 6, area A). The drainage network is similar to a rectilinear, but its tortuosity becomes greater as the slope inclination decreases and the slope stability increases (compare "Talus I" and "Talus II" vs. "Talus III" and "Talus IV" in Figure 6). The "Talus I" slope lateral parts are layered, explaining the formation sequences of distinct depressions (gutters) followed by infilling with fine-grained, weathered material. This interpretation is supported by the considerable slope inclination of 25–28°, substantial surficial water drainage, the occurrence of snow-mud avalanches and landslides, as well as increased activity of the active permafrost layer. Moist, fine-grained material is deposited along the talus slope axis, while coarse weathered material is moved from the center of the slope to its marginal parts (Figure 6, area C). Most talus surface area is fresh blockfield (Figure 6). Plant succession partly covering debris and solifluction lobes started before the mid-1980s [44]). The "frontal" part of the talus cone is not recorded in the transverse GPR profile located upslope.

By analyzing the transverse and longitudinal views of the profiles and applying variable setting parameters of the measuring device, repeated reflection horizons were obtained at maximum depths of 25–30 m in the area of maximum debris accumulation in the central section of the "active" cones "Talus II" and "Talus III", and at a depth of about 15 m on the "stabilized" "Talus IV". The thickness of the taluses is in line with the results obtained by [46,47] on the slopes on the eastern side of Fugleberget (20–25 m) and the western slope of Fannytoppen (30–35 m) and is a slightly thinner (8–20 m) than taluses of Revdalen [48]. The active nowadays talus slopes are thicker, which may be related to the different times of talus development initiation due to the progressive deglaciation in the Hornsund region [48]. The thickness and activity of the Fugleberget talus slopes increase eastwards in the direction of deglaciation in the Holocene 3500–2000 years BP [49].

The diversification of the talus slopes' morphological activity is also referred to their location concerning the shoreline and their different inclinations. Talus cone stabilized under the greater influence of oceanic air masses has a decidedly smaller inclination. Here, we observe a faster rate of plant succession and the associated expansion of bird colonies established on the stabilized slopes (pers. comm. [50], Figure 6). These aspects impact the "stabilization" of gravitational origin's morphological processes and the emergence of the talus slope's final geometry with landslide and solifluction lobes (Figure 6, area B). A feature of "Talus IV" and "Talus III" is the greater thickness of the fine-grained deposits in the frontal part and the simultaneous overlapping of debris structures derived from weathering processes and the transport down the slope on the sediments of the marine terrace.

At the eastern foot of "Talus II", weathered deposits are seen as a highly reflective zone in the GPR profile. As in "Talus I", water-saturated sediment is settled in the middle of the cone (near the axis). The bedrock rises in the western part of "Talus II", and the weathered material becomes coarser. Owing to the greater slope inclination, "Talus II" is morphologically more active, implying shifting weathered material to "Talus III". Nevertheless, the westward rising bedrock and the less active "Talus III" promote weathered material's deposition at the boundary between "Talus II" and "Talus III", where the cones

merge. Such a layout may lead to the extension of "Talus II" (compare Figure 5a–c). Birkenmajer [25] described the overlap of sharp-edged weathering material on gravel marine deposits. Identification of the structure of the debris material, dead ice, and marine terrace sediment on the GPR profiles is consistent with the research results carried out on slopes in both polar and high-mountain areas [51–53]. The slightly inclined frontal part of the talus slope is where solifluction occurs. The lower part of stabilized "Talus IV" structure produces a model with the configuration shown in Figure 7.

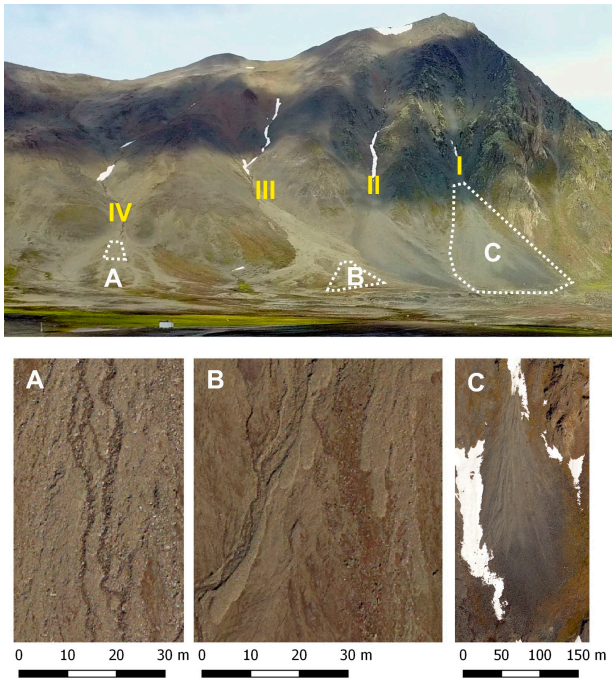

Figure 6. Selected morphological forms of the surface of Fugleberget talus cones (I–IV). Upper photo: green-gray fields of vegetation stabilizing "Talus III" and "Talus IV"; rockfields dominate on "Talus I" and "Talus II"; (**A**) gutters of surface drainage system; (**B**) landslides lobes; (**C**) "Talus I" with visible coarse-grained deposits on the marginal part of the cone (darker area). The upper panel is an oblique UAV photo taken on 29 August 2017 by D. Ignatiuk. The lower panel comprises orthomosaic fragments based on aerial photos taken on 22 June 2020 [45]). The areas shown on the bottom panel (**A**–**C**) have been marked on the upper UAV photo.

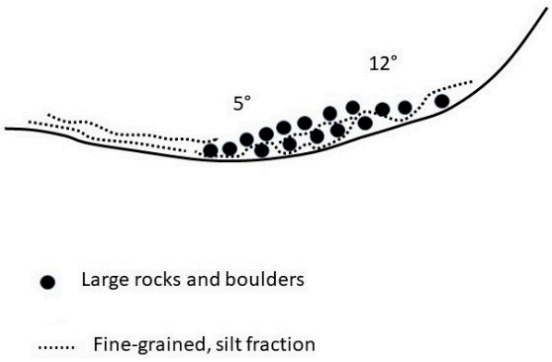

Figure 7. Diagram showing the morphometry and the structure of the lower part of talus slope based on GPR measurements and field observations.

4.2. Fugleberget Talus Slopes vs. Current Slope Classifications

The defined cone structure permits a comparison of its model to the functioning models of talus slopes developing under the periglacial climate's influence, described by French [23]. French models differ in the debris material's, inclination and structure on

particular talus slope sections. The structure of the lower part of the talus slope shown in Figure 7 is the closest to the free-face slope or pediment-like model presented in [23]. The rectilinear debris-mantled slope [23] has a similar inclination and a structure resembling the model based on the measurements on Fugleberget, but differences are visible in the frontal part, where the thickness is greater, and in the central part, where there is more mixed coarse-grained and fine-grained material.

A slightly different classification of slopes is presented by Ballantyne and Harris [24]. It includes four types of debris slopes: cliff and talus cone accumulation, rectilinear debris-mantled slope, convexo-concave slope characteristic of lowlands underlain by low bedrock, and stepped slope profile due to the development of cryoplanation terraces. Of the previously mentioned, the two first types are similar to the talus slope model recognized in this study.

The differences between the geometry obtained from the measurements and the literature model lie in the talus slope's extension. This is due to the transport of waste material to the frontal zone due to accelerating climate changes in the past 25 years [11], mainly permafrost thawing, increased liquid precipitation, and faster snow cover decay. Such relationships were described by French [23], Migoń [3], Herz et al. [54], and others. Piedmont-like slope form [23], however, is a classic example of a slope where the slight inclination indicates the dominance of solifluction processes. Such a fragment is visible on the frontal part of the Fugleberget mountainside, where the moderate inclination, fine rock material, and higher active layer temperature initiate creep.

4.3. Slopes Morphodynamics

The periglacial talus cones described in this paper are characterized by a low angle of inclination and, at the same time, high dynamics in the case of active slopes. It is a feature of talus cone built with an admixture of clay rocks, which are rounded, slightly rough, fine, absorbable, and washed with rain- and meltwater [23,55]. Under the influence of water, the angle of the slope decreases significantly. This is favored by other forms of movement, such as compaction, creeping, formation of landslide lobes, spreading of mud streams, and solifluction movement [14]. A critical element influencing the movement of the weathered cover along the Spitsbergen slopes is the modern process of increasing the thickness of the active layer [8,9], which causes the presence of vertical movements, i.e., increased dynamics of debris deposition in the summer and their ascending during the freezing of the active layer. This results in large rock aggregates at the top of the cone and deposition of fine fractions at the bottom. Such a phenomenon may also result from ground ice bonding the upper parts of the slope [55]. Most studies on the dynamics of debris cones are associated with perennial permafrost or seasonal ice thawing [56].

Having analyzed the geometry and structure of the active talus slopes ("Talus I" and "Talus II"), one can assume that they will attain the model observed in the "Talus IV" in the next phase of evolution.

4.4. Climatic Determinants for the Contemporary Slope Activity

The development of slopes depends on the environmental conditions related to the morphology of the slope, the supply of material, and its redeposition. The lithology of rockwall and the range of the alimentation area affect the erosion rate and the supply of weathered sediment [46]. Factors influencing the instability of the slope, such as slope inclination, the thickness and cohesiveness of the weathered material, and the presence of water, are important for the further movement of the material. Mass movements take the form of debris flows, slush streams, avalanche events, landslides, and solifluction flows. Extreme weather events related to rapid precipitation, snow melting, and a combination of both factors play a special role in triggering the dislocation of weathered material [57,58]. In Svalbard, debris flows on the slopes are repeated every 80–500 years, and the slush avalanche every 500 years [57]. Dendrochronological studies on talus cones at Wedel Jarlsberg Land show that contemporary debris flows correlate with the seasons characterized by extreme

summer rainfall 1994 and 1996 [59]. Similar results were obtained in the "Talus I" area, characterized by poor colonization of dwarf shrubs, the oldest collected specimens from the 1970s [44]. The colonization process proves the weakening of the morphological activity of the slope in the 1980s and its intensification in the 1990s, as well as the constant supply of fresh deposit material [44].

Contemporary climate change contributes to the increase in slope activity. Based on meteorological data from Hornsund [12,60,61], it can be concluded that since the late 1970s, the number of extreme and intense rainfalls has been increasing over time, also including the summer months (Figure 8). The 1990s (and especially 1994, 1996, 1999) were characterized by the highest number of rainfall days belonging to the top 5% of the days with the highest rainfall intensity (more than 7 mm per day). The increase in the number of days with maximum summer rainfall is accompanied by an increase in temperature in May–June (Figure 8), contributing to more rapid thaw periods and a more intensive water supply. The sum of positive degree days (PDDs) from May to June has been increasing at a rate of 14.9 PDD per decade since the late 1970s. The increase in temperature in the spring and autumn months [12] also translates into an extension of the period during the year in which precipitation occurs in liquid form, increasing rainwater's role in the slope development process. An additional factor that influences the instability of the slopes is the thickening of the active layer of permafrost. We can indirectly observe it in the rapid increase in ground temperature in Hornsund (Figure 4) as a response to the increase in air temperature in the summer months (Figure 8). The PDD sum July–September recorded at the Hornsund station in the last 40 years has grown at the rate of 34.1 PDD per decade. Extending the time when the temperature fluctuates around 0 °C and increasing the amount of water deposited in the ground is a significant factor activating and intensifying the frost weathering process. The increase in precipitation and the simultaneous deeper thawing of the soil results in the leaching of weathered material from the space between large rock blocks and its deposition at lower levels. The above-mentioned climatic indicators and their clear trends translate into an increase in instability and dynamics of slope processes on currently active talus slopes and a slower stabilization rate on cones colonized by tundra vegetation.

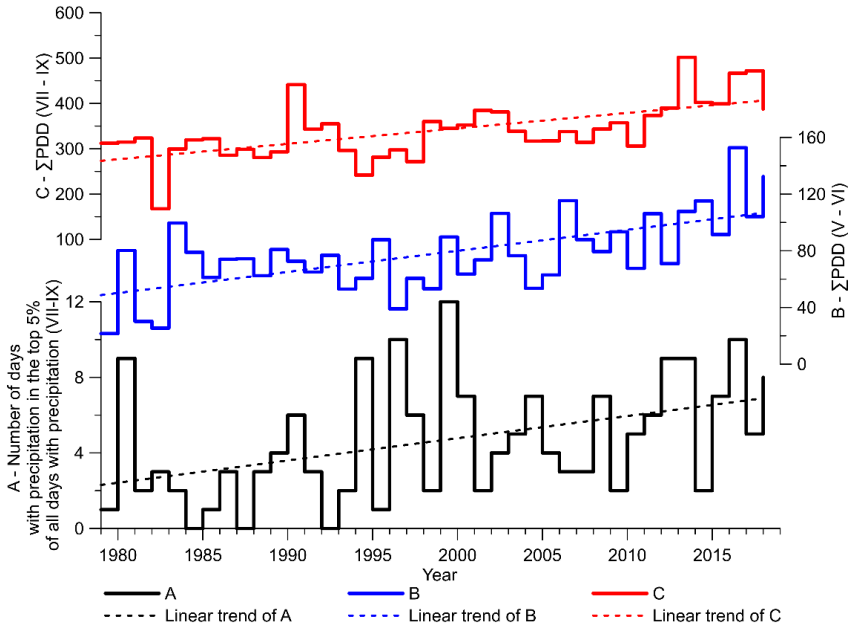

Figure 8. The number of days with precipitation in the top 5% of all days with precipitation in summer months VII–IV (**A**) and the sum of the positive degree days (PDD) in May–June (**B**) and July–September (**C**) observed at WMO meteorological Station in Hornsund [12]. Graphs based on fata series [62,63].

5. Conclusions

The following conclusions can be drawn from our results:

1. The thickness of the weathered material achieved a maximum of 25–30 m on the morphologically active slopes and 15 m on the stabilized slope.
2. The stabilized slope is manifested by advanced plant succession.
3. There was a tendency towards a slight but systematic growth in the thickness of the debris cover, consisting of fine rock material in the "frontal" part of the talus deposit.
4. According to the talus slopes' observed structure, sharp-edged weathering material derived from the slopes overlapped the marine terrace's sediment.
5. The structure diagrams of the talus slopes observed in the field and based on GPR profiles' interpretation are similar to the compilation of models, known in the literature as convexo-concave debris-mantled slopes and pediment-like forms [24,46].
6. The data from the end of the 1970s show that the climatic indicators contributing to the instability of the slopes and the activation of mass movements on talus cones, such as the frequency of extreme summer rainfalls, the sum of PDD both during the melting of the snow cover (May–June), as well as in the period of permafrost thawing (July–September) show an upward trend.

Author Contributions: Conceptualization, P.D.; methodology, P.D. and M.G.; investigation, P.D. and M.G.; data curation, P.D. and M.G.; writing—original draft preparation, P.D. and M.G.; writing—review and editing, P.D. and M.G.; visualization, P.D. and M.G.; funding acquisition, P.D. and M.G. All authors have read and agreed to the published version of the manuscript.

Funding: This research received funding from the projects Arctic climate system study of ocean, sea ice and glacier interactions in the Svalbard area—AWAKE2 (Pol-Nor/198675/17/2013) and has been supported from the funds of the Leading National Research Centre (KNOW) received by the Centre for Polar Studies for the period 2014–2018.

Institutional Review Board Statement: Not applicable.

Data Availability Statement: The GPR data presented in this study are openly available in the Polish Polar Data Base repository: https://ppdb.us.edu.pl/geonetwork/srv/eng/catalog.search#/metadata/0de61407-13d2-4369-93f0-77423b8a9b9f (accessed on 28 October 2021).

Acknowledgments: The studies were carried out as part of the scientific activity of the Centre for Polar Studies (University of Silesia in Katowice) with the use of research and logistic equipment (GPR set, GNSS receivers, snowmobiles and supporting equipment) of the Polar Laboratory of the University of Silesia in Katowice. The authors wish to thank the Institute of Geophysics Polish Academy of Sciences for access to the meteorological data from the Polish Polar Station weather station (available at: https://monitoring-hornsund.igf.edu.pl, (accessed on 29 October 2021)) used in the introduction and for making the 30 MHz RTA antenna available for research. We would like to thank Michał Laska (the University of Silesia in Katowice) for support during the GPR survey and Michał Pętlicki for sharing the results of the TLS and DEM in the Fugleberget area, which was used in the description of the cone geometry, and for his help in preparing the methodological description of TLS measurements. We would like to thank Dariusz Ignatiuk, Leszek Kolondra, Małgorzata Błaszczyk and Michał Laska for providing UAV, aerial and orthophoto imageries. The Polish Polar Station Hornsund ensured logistic facilities during the field campaign as well as support from the station staff during field research. The authors acknowledge the three anonymous reviewers for their valuable comments.

Conflicts of Interest: The authors declare no conflict of interest. The funders had no role in the design of the study; in the collection, analyses, or interpretation of data; in the writing of the manuscript, or in the decision to publish the results.

References

1. Łoziński, W. Die periglaziale Fazies der mechanischen Verwitterung. In Proceedings of the 11th International Geological Congress, Stockholm, Sweden, 1 January 1910; Volume 1912, pp. 1039–1053.
2. Ballantyne, C.K. A general model of paraglacial landscape response. *Holocene* **2002**, *12*, 371–376. [CrossRef]
3. Migoń, P. *Geomorfologia*; PWN: Warszawa, Poland, 2009; pp. 108–142. (In Polish)
4. Everdigen, R.O. *Multi-Language Glossary of Permafrost and Related Ground-Ice Terms. Definitions*; The University of Calgary: Calgary, AB, Canada, 1998; pp. 62–63.
5. Luckman, B.H. Talus slopes. In *The Encyclopedia of Quaternary Science*; Elias, S.A., Ed.; Elsevier: Amsterdam, The Netherlands, 2013; pp. 556–573.
6. French, H.M. *The Periglacial Environment*, 4th ed.; John Wiley & Sons: Hoboken, NJ, USA; Chichester, UK, 2018; p. xxii+515.
7. Büdel, J. Die Klima-morphologischen Zonen der Polarländer: Beiträge Zur Geomorphologie Der Klimazonen Und Vorzeitklimate II. *Erdkunde* **1948**, *2*, 22–53. [CrossRef]
8. IPCC 2018. *Climate Change: Impacts, Adaptation and Vulnerability*; The IPCC Third Assessment Report; Cambridge University Press: Cambridge, UK; New York, NY, USA, 2001.
9. Dolnicki, P. *Charakterystyka Warstwy Czynnej Wieloletniej Zmarzliny na Spitsbergenie, Svalbard (na Przykładzie Równiny Nadmorskiej Fuglebergsletta, Hornsund)*; Wydawnictwo Uniwersytetu Pedagogicznego: Kraków, Poland, 2020. (In Polish)
10. Repelewska-Pękalowa, J.; Pękala, K. Reakcja wieloletniej zmarzliny na zmiany klimatu. In *Zmiany Klimatyczne w Arktyce i Antarktyce w Ostatnim Pięćdziesięcioleciu XX Wieku i ich Implikacje Środowiskowe*; Styszyńska, A., Marsz, A.A., Eds.; Akademia Morska: Gdynia, Poland, 2007; pp. 279–288. (In Polish)
11. Łupikasza, E. Zmienność występowania opadów deszczu i śniegu w Hornsundzie w okresie lipiec 1978–grudzień 2002. *Problemy Klimatologii Polarnej* **2003**, *13*, 93–105. (In Polish)
12. Osuch, M.A.; Wawrzyniak, T. 40-year High Arctic climatological dataset of the Polish Polar Station Hornsund (SW Spitsbergen, Svalbard). *Earth Syst. Sci. Data* **2020**, *12*, 805–815. [CrossRef]
13. Thiedig, F.; Kresling, A. Meteorologische und geologische Bedingungen bei der Entstehung von Muren im Juli 1972 auf Spitzbergen. *Polarforschung* **1973**, *43*, 40–49.
14. Rapp, A. Slope erosion due to extreme rainfall, with examples from tropical and arctic mountains. *Math.-Phys. Kl.* **1974**, *29*, 40–49.
15. Jahn, A. Quantitative analysis of periglacial processes in Spitsbergen. In *Nauki o Ziemi*; Uniwersytet Wrocławski, Zeszyty Naukowe Series B. No. 5: Krakow, Poland, 1961; pp. 1–54.
16. De Haas, T.; Kleinhans, M.G.; Carbonneau, P.E.; Rubensdotterc, L.; Hauber, E.G. Surface morphology of fans in the high-Arctic periglacial environment of Svalbard. Controls and processes. *Earth Sci. Rev.* **2015**, *146*, 163–182. [CrossRef]
17. Akerman, J. Relations between slow slope processes and active-layer thickness 1972–2002, Kapp Linné, Svalbard. *Nor. J. Geogr.* **2005**, *59*, 116–128. [CrossRef]
18. Rączkowska, Z. Współczesna rzeźba peryglacjalna wysokich gór Europy. *Prace Geograficzne IGiPZ PAN* **2007**, *212*, 65–70. (In Polish)
19. Rączkowska, Z. Zróżnicowanie współczesnej rzeźby peryglacjalnej w górach wysokich Europy. *Landf. Anal.* **2008**, *9*, 120–122. (In Polish)
20. Van Steijn, H.; de Ruig, J.; Hoozemans, F. Morphological and mechanical aspects of debris flows in parts of the French Alps. *Z. Geomorphol.* **1988**, *32*, 143–161. [CrossRef]
21. Halles, T.C.; Roering, J.J. Climatic–controlled variations in scree production, Southern Alps, New Zealand. *Geology* **2005**, *33*, 701–704. [CrossRef]
22. Moore, J.R.; Sanders, J.W.; Dietrich, W.E.; Glaser, S.D. Influence of rock mass strength on the erosion rate of alpine cliffs. *Earth Surface Process. Landf.* **2009**, *34*, 1339–1352. [CrossRef]
23. French, H.M. *The Peryglacial Environment*, 3rd ed.; Wiley and Sons: Hoboken, NJ, USA, 2007; Online Book; Available online: https://onlinelibrary.wiley.com/doi/book/10.1002/9781118684931 (accessed on 1 April 2021).
24. Ballantyne, C.K.; Harris, C. *The Periglaciation of Great Britain*; Cambridge University Press: Cambridge, UK, 1994; p. 330.
25. Birkenmajer, K.; Jania, J.; Pulina, M. Hornsund, Spitsbergen. In *Geologia, 1:75000 (Mapa z Objaśnieniem)*; Uniwersytet Śląski: Katowice, Poland, 1991. (In Polish)
26. Martini, A. Contemporary periglacial weathering processes of the mountain massifs in the vicinity of Hornsund, SW Spitsbergen. *Acta Univ. Wratislawiensis* **1986**, *966*, 45–73.
27. Werenskioldbreen and Surrounding Areas. *Spitsbergen, Svalbard, Norway. Ortophotomap 1:25,000*; Jania, J., Kolondra, L., Aas, H.F., Eds.; Uniwersytet Śląski: Katowice, Poland; Norsk Polarinstitutt: Tromsø, Norway, 2002.
28. Czeppe, Z. Przebieg głównych procesów morfogenetycznych w południowo-zachodnim Spitsbergenie. *Zesz. Nauk. Uniw. Jagiellońskiego* **1966**, *13*, 125. (In Polish)
29. Głowicki, B. Radiation conditions in the Hornsund area (Spitsbergen). *Pol. Polar Res.* **1985**, *6*, 331–339. [CrossRef]
30. Niedźwiedź, T. The main factors forming the climate of the Hornsund (Spitsbergen). *Zeszyty Naukowe UJ—Prace Geograficzne* **1993**, *94*, 49–63.
31. Marsz, A.; Styszyńska, A. *Climate and Climate Change at Hornsund, Svalbard*; Publishing House Gdynia Maritime Academy: Gdynia, Poland, 2013; p. 402.

32. Niedźwiedź, T. Wpływ cyrkulacji atmosfery na wysokie opady w Hornsundzie (Spitsbergen). *Probl. Klimatol. Polarn.* **2002**, *12*, 65–75. (In Polish)
33. Leszkiewicz, J.; Głowacki, P. Metamorfoza pokrywy śnieżnej w rejonie południowego Spitsbergenu w sezonie 1992/1993. *Probl. Klimatol. Polarn.* **2001**, *11*, 41–54. (In Polish)
34. Sass, O. Determination of the internal structure of alpine talus deposits using different geophysical methods (Lechtaler Alps, Austria). *Geomorphology* **2006**, *80*, 45–58. [CrossRef]
35. Sass, O. Bedrock detection and talus thickness assessment in the European Alps using geophysical methods. *J. Appl. Geophys.* **2007**, *62*, 254–269. [CrossRef]
36. Otto, J.C.; Sass, O. Comparing geophysical methods for talus slope investigations in the Turtmann valley (Swiss Alps). *Geomorphology* **2006**, *76*, 257–272. [CrossRef]
37. Sass, O.; Krautblatter, M. Debris flow-dominated and rockfall-dominated talus slopes: Genetic models derived from GPR measurements. *Geomorphology* **2007**, *86*, 176–192. [CrossRef]
38. Schrott, L.; Sass, O. Application of field geophysics in geomorphology: Advances and limitations exemplified by case studies. *Geomorphology* **2008**, *93*, 55–73. [CrossRef]
39. Gądek, B.; Grabiec, M.; Kędzia, S. Rzeźba i wybrane element klimatu najwyżej położonych cyrków polodowcowych na przykładzie Koziej Dolniki. *Prace Geograficzne* **2013**, *239*, 49–56.
40. Micheletti, N.; Tonini, M.; Lane, S.N. Geomorphological activity at a rock glacier front detected with a 3D density-based clustering algorithm. *Geomorphology* **2017**, *278*, 287–297. [CrossRef]
41. Pfeiffer, J.; Zieher, T.; Bremer, M.; Wichmann, V.; Rutzinger, M. Derivation of Three-Dimensional Displacement Vectors from Multi-Temporal Long-Range Terrestrial Laser Scanning at the Reissenschuh Landslide (Tyrol, Austria). *Remote Sens.* **2018**, *10*, 16–88. [CrossRef]
42. Gabbud, C.; Micheletti, N.; Lane, S.N. Lidar measurement of surface melt for a temperate Alpine glacier at the seasonal and hourly scales. *J. Glaciol.* **2015**, *61*, 963–974. [CrossRef]
43. Pętlicki, M. Subglacial Topography of an Icefall Inferred from Repeated Terrestrial Laser Scanning. *IEEE Geosci. Remote Sens. Lett.* **2018**, *15*, 1461–1465. [CrossRef]
44. Owczarek, P. Talus cone activity recorded by tree-rings of Arctic dwarf shrubs: A study case from SW Spitsbergen, Norway. *Geologija* **2010**, *52*, 34–39. [CrossRef]
45. Błaszczyk, M.; Laska, M.; Sivertsen, A.; Jawak, S.D. Combined use of aerial photogrammetry and terrestrial laser scanning for detecting geomorphological changes in Hornsund, Svalbard. *Remote Sens.* **2022**, *14*, 601. [CrossRef]
46. Senderak, K.; Kondracka, M.; Gądek, B. Talus slope evolution under the influence of glaciers with the example of slopes near the Hans Glacier, SW Spitsbergen, Norway. *Geomorphology* **2017**, *285*, 225–234. [CrossRef]
47. Senderak, K.; Kondracka, M.; Gądek, B. Postglacial talus slope development imaged by the ERT method: Comparison of slopes from SW Spitsbergen, Norway and Tatra Mountains, Poland. *Open Geosci.* **2019**, *11*, 1084–1097. [CrossRef]
48. Senderak, K.; Kondracka, M.; Gądek, B. Processes controlling the development of talus slopes in SW Spitsbergen. The role of deglaciation and periglacial conditions. *Land Degrad Dev.* **2021**, *32*, 208–222. [CrossRef]
49. Lindner, L.; Pękala, K. Quaternary glaciations of South Spitsbergen and their correlation with Scandinavian glaciations of Poland. *Acta Gaologlea Polonica* **1983**, *33*, 169–182.
50. Kulaszewicz, I.; (University of Gdansk, Poland). Personal communication, 2016.
51. Grabiec, M. *Stan i Współczesne Zmiany Systemów Lodowcowych Południowego Spitsbergenu w Świetle Badań Metodami Radarowymi*; Wydawnictwo Uniwersytetu Śląskiego: Katowice, Poland, 2017.
52. Dolnicki, P.; Grabiec, M.; Puczko, D.; Gawor, Ł.; Budzik, T.; Klementowski, J. Variability of temperature and thickness of permafrost active layer at coastal sites of Svalbard. *Pol. Polar Res.* **2013**, *34*, 353–374. [CrossRef]
53. Gądek, B.; Grabiec, M.; Kędzia, S.; Rączkowska, Z. Reflection of climate changes in the structure and morphodynamics of talus slopes (the Tatra Mountains, Poland). *Geomorphology* **2016**, *263*, 39–49. [CrossRef]
54. Herz, T.; King, L.; Gubler, H. Microclimate within coarse debris of talus slopes in the alpine periglacial belt and its effect on permafrost. In Proceedings of the 8th International Conference on Permafrost; IPA: Zurich, Switzerland, 2003; pp. 383–388.
55. Traczyk, A.; Korabiewski, B. *Pełznięcie pokryw gruzowych na stokach Fugleberget w Hornsundzie (SW Spitsbergen), In Środowisko Przyrodnicze Obszarów Polarnych*; Kowalska, A., Latocha, A., Marszałek, H., Pereyma, J., Eds.; Uniwersytet Wrocławski: Wroclaw, Poland, 2008; pp. 89–95. (In Polish) [CrossRef]
56. Pisabarro, A.; Pellitero, R.; Serrano, E.; Gómez-Lende, M.; Gonzalez-Trueba, J.J. Ground temperatures, landforms and processes in an Atlantic mountain. Cantabrian Mountains (Northern Spain). *Catena* **2017**, *149*, 623–636. [CrossRef]
57. André, M.F. Holocene Climate Fluctuations and Geomorphic Impact of Extreme Events in Svalbard. *Geografiska Annaler. Ser. A Phys. Geogr.* **1995**, *77*, 241–250. [CrossRef]
58. Rebetez, M. *Climatic Change and Debris Flows in High Mountain Regions: The Case Study of The Ritigraben Torrent (Swiss Alps)*; Springer: Berlin/Heidelberg, Germany, 1997; Volume 36, pp. 371–389.
59. Owczarek, P.; Laatocha, A.; Wistuba, M.; Malik, I. Reconstruction of modern debris flow activity in the arctic environment with the use of dwarf shrubs (south-western Spitsbergen)—A new dendrochronological approach. *Zeitschrift für Geomorphologie* **2013**, *57*, 75–95. [CrossRef]

60. Łupikasza, E. Long-term variability of extreme precipitation in Hornsund (Spitsbergen) and their relation with atmospheric circulation. *Probl. Klimatol. Polarn.* **2007**, *17*, 87–103.
61. Łupikasza, E. Change in precipitation intensity in Hornsund (Spitsbergen) in the 1978–2008 period. *Problemy Klimatologii Polarnej* **2009**, *19*, 169–188.
62. Wawrzyniak, T.; Osuch, M. *Daily Precipitation (1979–2018) at the Arctic Meteorological Station Hornsund, Spitsbergen*; PANGAEA: Bremen, Germany, 2019. [CrossRef]
63. Wawrzyniak, T.; Osuch, M. *Daily Mean Air Temperature (1979–2018) at the Arctic Meteorological Station Hornsund, Spitsbergen*; PANGAEA: Bremen, Germany, 2019. [CrossRef]